Article

An Empirical Algorithm for Estimating Agricultural and Riparian Evapotranspiration Using MODIS Enhanced Vegetation Index and Ground Measurements of ET. I. Description of Method

Pamela L. Nagler [1,*], Kiyomi Morino [2], R. Scott Murray [3], John Osterberg [4] and Edward P. Glenn [3]

[1] US Geological Survey, Southwest Biological Science Center, Sonoran Desert Research Station, 1110 E. South Campus Drive, Room 123, Tucson, AZ 85721, USA

[2] Laboratory of Tree Ring Research, 105 West Stadium, University of Arizona, Tucson, AZ 85721, USA; E-Mail: kmorino@lttr.arizona.edu

[3] Environmental Research Laboratory, University of Arizona, 2601 East Airport Drive, Tucson, AZ 85706, USA; E-Mails: rsmurray@email.arizona.edu (S.M.); eglenn@ag.arizona.edu (E.G.)

[4] US Bureau of Reclamation, Denver Federal Center, Denver, CO 80225, USA; E-Mail: josterberg@do.usbr.gov

* Author to whom correspondence should be addressed; E-Mail: pnagler@usgs.gov.

Abstract: We used the Enhanced Vegetation Index (EVI) from MODIS to scale evapotranspiration (ET_{actual}) over agricultural and riparian areas along the Lower Colorado River in the southwestern US. Ground measurements of ET_{actual} by alfalfa, saltcedar, cottonwood and arrowweed were expressed as fraction of potential (reference crop) ET_o (ET_oF) then regressed against EVI scaled between bare soil (0) and full vegetation cover (1.0) (EVI*). EVI* values were calculated based on maximum and minimum EVI values from a large set of riparian values in a previous study. A satisfactory relationship was found between crop and riparian plant ET_oF and EVI*, with an error or uncertainty of about 20% in the mean estimate (mean $ET_{actual} = 6.2$ mm d^{-1}, RMSE = 1.2 mm d^{-1}). The equation for ET_{actual} was: $ET_{actual} = 1.22 \times ET_{o\text{-}BC} \times EVI*$, where $ET_{o\text{-}BC}$ is the Blaney Criddle formula for ET_o. This single algorithm applies to all the vegetation types in the study, and offers an alternative to ET_{actual} estimates that use crop coefficients set by expert

opinion, by using an algorithm based on the actual state of the canopy as determined by time-series satellite images.

Keywords: sap flux; transpiration; stomatal conductance; evaporative fraction; remote sensing; saltcedar

---

1. Introduction

1.1. The Vegetation Index Approach for Scaling ET by Remote Sensing

Recent studies have combined ground measurements of evapotranspiration (ET), meteorological variables, and vegetation indices (VIs) determined by satellite sensors to project plant water use over diverse biomes, including deserts [1,2], semiarid rangelands [3], agricultural districts [4-6], riparian corridors [7,8], rainforests [9], and mixed landscape units at regional [10,11] and global [12,13] scales of measurement. Unlike remote sensing methods based on thermal (NIR) bands on Landsat or other high-resolution satellites, which provide a snap-shot of actual ET (ET_{actual}) at the time of satellite overpass [14,15], VI methods are useful in projecting ET_{actual} over longer time periods (weeks, months and years), due to the modulated response of VIs to environmental conditions. These methods use time-series images from frequent-return sensor systems such as the Moderate Resolution Imaging Spectrometer (MODIS) on the Terra satellite [16,17].

VI methods work due to the high correlation between plant transpiration and green foliage density measured by VIs [16,17]. Unlike thermal-band methods, VI methods cannot estimate the direct evaporation component of ET_{actual} [6]. However, in many biomes, plant transpiration dominates ET_{actual}, and is often the major unknown in wide-area water budgets. In arid zone phreatophyte communities, as studied here, plants withdraw water from the underlying aquifer, precipitation is low, and the top meter of soil is often dry [1,7,8]. Bare soil evaporation is often a small term in the water budget of these systems.

Although many variations exist, most of the methods are based on initial observations by Choudhury *et al.* [18] who showed that crop transpiration on a ground area basis (E_G) can be calculated as:

$$E_G = ET_o \times k \times VI^*$$

(1)

where ET_o is daily potential or reference crop ET determined from micrometeorological data from one of several possible methods, VI^* is one of several possible VIs scaled between 0 (no vegetation) and 1 (full cover vegetation), and k is a constant determined by linear regression of measured E_G with VI^* over a crop cycle. Equation (1) can be rearranged to give the evaporative fraction ($E_G F$), the ratio of E_G to ET_o:

$$ET_o F = E_G / ET_o = k \times VI^*$$

(2)

$ET_o F$ can then be used to scale E_G (e.g., from sap flow sensors) or ET_{actual} (e.g., from moisture flux towers) over wider areas and longer time spans than encompassed by the initial calibration measurements, if ET_o and VI^* scaling data are available. The term kVI^* replaces the empirically-

derived crop coefficient (k_c) normally used in Equation 1 [6,19] with a parameter based on the actual state of the canopy. Properly calibrated, Equation 1 can predict crop ET_{actual}. For example, Hunsaker *et al.* [4] found that wheat ET_{actual} predicted from ET_o and NDVI was within 5% of values determined in a weighing lysimeter. Gonzalez-Dugo *et al.* [6] compared a VI/crop coefficient remote sensing method for estimating ET_{actual} of corn and soybean crops in central Iowa, US, with three Surface Energy Balance (SEB) methods that utilized thermal bands, and reported root mean square differences of 0.4 mm d^{-1} for the VI/crop coefficient method and 0.4–0.6 mm d^{-1} for SEB methods when compared to moisture flux tower measurements.

1.2. Potential Problems in Applying VI Methods to Arid Zone Plant Communities

VI methods based on Equations 1 and 2 assume a fixed, or at least a predictable, relationship between green foliage density and plant transpiration on daily or longer time steps under a given set of environmental conditions [1,18]. This is often true for unstressed vegetation such as irrigated crops [19]. However, the applicability of Equation 1 to natural stands of plants can be questioned, because it cannot be assumed that they are growing under unstressed conditions [20]. This is especially true of arid zone plants. Due to heat, water stress and nutrient limitations, desert plants often exhibit midday depression of transpiration and stomatal conductance even under full canopy conditions [21]. Mata-Gonzalez *et al.* [20] estimated that crop coefficient methods based on ET_o and leaf area index (LAI) of desert plants might over-estimate ET_{actual} by 23–100%. It is sometimes possible to recalibrate ET_{actual} estimates of natural plant stands to account for reduced stomatal conductance based on soil moisture content, precipitation, vapor pressure deficit, or depth to the water table, but the range of conditions under which plants grow in natural settings is very large and difficult to estimate by remote sensing.

1.3. Goal and Objectives

The goal of the present study was to develop and validate a remote sensing method to monitor E_G or ET_{actual} over mixed riparian and agricultural areas along the Lower Colorado River in the US, to resolve uncertainties in the role of riparian E_G in water budgets of saltcedar-dominated rivers [22-32]. These districts are often mixed landscapes of riparian vegetation and agricultural fields, so a robust remote sensing method that can project E_G or ET_{actual} over different plant types is needed for monitoring water consumption.

To accomplish the goal, we developed algorithms based on Equations 1 and 2 relating E_G or ET_{actual} to the Enhanced Vegetation Index (EVI) from the MODIS sensors on the Terra satellite [33]. We measured transpiration (E) and stomatal conductance (G_S) of saltcedar with sap flow sensors in six dense saltcedar stands at Cibola National Wildlife Refuge (CNWR) on the Lower Colorado River. Three of the sites were measured in 2007 and were reported in [8] and three additional sites were measured in 2008 and are reported here. Transpiration was measured on a leaf-area basis (E_L), then projected to canopy-area (E_C) and ground-area (E_G) measurements by determining leaf area index (LAI) for each study plot. Plant stress was evaluated by diurnal responses of E_L and G_S to meteorological variables at each site. To extend our method to agricultural crops, we measured ET_{actual} of irrigated alfalfa in an adjacent irrigation district, based on soil moisture depletion measured with a

neutron hydroprobe. We then combined saltcedar and alfalfa data with ET_{actual} or E_G data from other sites and species on the Lower Colorado River to scale riparian and agricultural ET over annual cycles using the Penman Monteith and Blaney Criddle equations for calculating ET_o. Errors and uncertainties in the ET_{actual} algorithms are discussed, and compared to other remote sensing methods for ET_{actual} estimation.

2. Methods

2.1. Site Description

CNWR is located near Blythe, CA, on the Lower Colorado River [8,34]. This is an extreme, low-desert environment. Annual rainfall is under 100 mm yr^{-1}, occurring as occasional winter rains augmented by summer monsoon rains in July and August [35]. The hottest month of the year is August with an average maximum daily temperature of 38 °C and the coolest month is December with an average minimum daily temperature of 4 °C.

Names and locations of measurement sites and soil and aquifer conditions are in Table 1. Sites were given fanciful names based mainly on summer working conditions. Saltcedar study sites were on a floodplain terrace in six plots established at different distances from the active channel of the river (Figure 1). These plots were established by the US Bureau of Reclamation and a consortium of universities with the purpose of developing ET_{actual} estimation methods for western US rivers [7,34]. Three of the sites were equipped with Bowen ratio flux towers but data from the towers are not yet available for comparison with sap flow results. Sap flow measurements for Swamp, Slitherin and Diablo East were reported in Nagler *et al.* [8] and Hot Springs, Diablo Tower, and Diablo Southwest are reported here. Each plot contained one to five observation wells to measure depth and salinity of the aquifer. The Hot Springs site was on the edge of a bare area in which geothermal water approached within 2.5 m of the surface. Saltcedar was the dominant plant at each site, growing in dense stands interrupted by areas of light, sandy soil, with occasional arrowweed (*Pluchia sericea*) and quailbush (*Atriplex lentiformis*) shrubs and stunted screwbean mesquite (*Prosopis pubescens*) trees occurring in the more open areas. Methods for determining soil and aquifer properties, summarized in Table 1, are described in Nagler *et al.* [8,34]. Depth to the aquifer and salinity of the aquifer were measured at monthly intervals from 2007–2008. Soil properties were determined at 0.3 m intervals in auger holes bored from the surface to the top of the aquifer at each site in 2008 as described in [34]. Alfalfa ET_{actual} was measured in a well-managed field (Hayday Farms, Inc., Blythe, CA) within the floodplain of the river, approximately 8.4 km from the active channel, in the Palo Verde Irrigation District adjacent to CNWR. The field was 375 m by 815 m (30.1 ha) in area. Bowen ratio and eddy covariance moisture flux towers were installed in the middle of the field, as part of the Bureau of Reclamation ET_{actual} monitoring program. The field was flood-irrigated at ca. 10 day intervals and cut each 30 days in summer, but less frequently in winter.

Table 1. ET$_{actual}$ measurement sites for saltcedar and alfalfa on the Lower Colorado River. ET$_{actual}$ for alfalfa and for saltcedar at Diablo SW, Diablo, and Hot Springs were measured in the present study. Data for Swamp, Slitherin and Diablo East were from [7]. Soil texture data are % sand (S), silt (Si) and clay (C). Numbers in parentheses are standard errors of means.

Site	Lat/Lon (º North, º West)	Distance From River (m)	Soil Texture (S-Si-Cl)	Depth to Aquifer (m)	Aquifer Salinity (dS m^{-1})	Aquifer Temperature (ºC)
Swamp	33.2754, 114.6873	200	25-55-20	2.35 (0.03)	3.90 (0.18)	23.1 (0.3)
Slitherin	33.2746, 114.7098	750	40-45-15	3.51 (0.06)	4.72 (0.48)	22.5 (0.2)
Diablo Tower	33.2659, 114.6992	1500	50-35-15	2.61 (0.06)	15.49 (0.18)	22.8 (0.3)
Diablo Southwest	33.2663, 114.7002	1550	90-7-3	2.79 (0.06)	24.0 (0.55)	22.2 (0.2)
Diablo East	33.2687, 114.6895	870	95-2-3	2.40 (0.04)	7.1 (0.19)	24.9 (0.2)
Hot Springs	33.2783, 114.6924	557	85-10-5	2.36 (0.03)	5.39 (0.07)	51.0 (0.5)
Hayday Farms Alfalfa	33.4683, 114.6938	8,439	-	1.81 (0.05)	1.85 (0.05)	23.0 (0.35)

Figure 1. Sap flow measurement sites for saltcedar at Cibola National Wildlife Refuge. SL = Slitherin; HS = Hot Springs; SW = Swamp; DT = Diablo Tower; DSW = Diablo Southwest; DE = Diablo East.
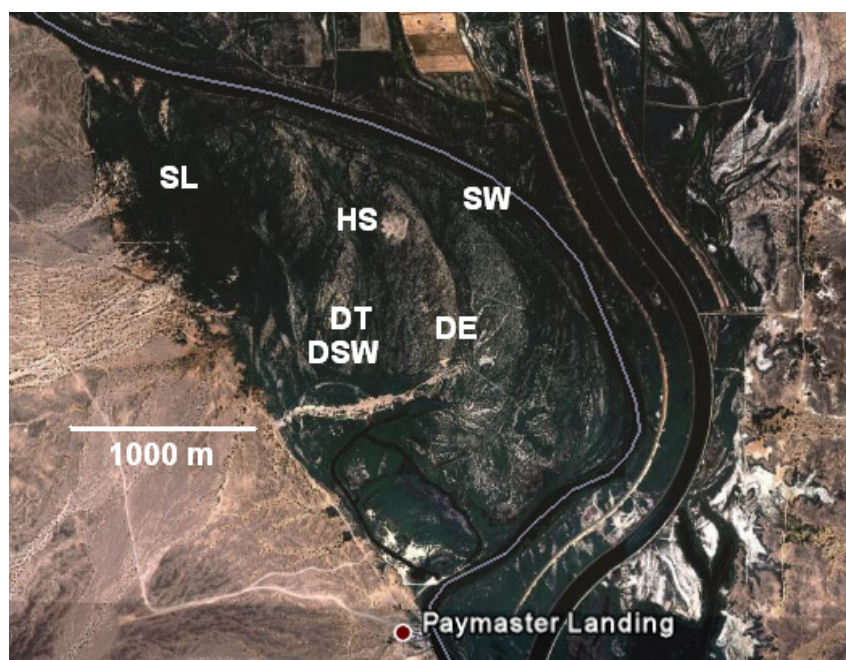
2.2. Sap Flow Measurements

Sap flow was measured by the tissue-heat-balance method as described in Sala *et al.* [31], Grime and Sinclair [36], Kjelgaard *et al.* [37] and Nagler *et al.* [8,38,39]. We used home-made sensors described in Scott *et al.* [40], which were field-validated by measurements of ET_{actual} by flux towers [40]. In the tissue-heat-balance method, an intact branch containing leaves is wrapped by a heating wire and a constant source of low-grade heat is applied to the branch. Thermocouples embedded in the branch measure temperatures upstream and downstream from the heat source, and a thermopile outside the heating wire in the surrounding layer of insulation measures heat lost radially from the branch. A heat balance equation is then solved to calculate heat transported by convection in the transpiration stream, and the results are expressed in terms of grams of water transported per hour. Diurnal patterns of transpiration were combined with diurnal patterns of atmospheric water demand as measured by vapor pressure deficit (D) to calculate stomatal (canopy) conductance (G_S) [41,42].

Branches ranged from 5 mm to 15 mm in diameter. The sensors and thermopile were wrapped in insulating foam and covered with reflective foil to minimize solar heating. An instrument station containing a solar panel, four 6 volt batteries, one to three multiplexers, a voltage regulator, and a data-logger was established in each plot. A computer program transformed temperature data from the sensors into sap flow rate per hour. This program also filtered the data to remove aberrant values. The sensor readings were processed with a Matlab (MathWorks, Inc., Natick, MA) script composed by us.

In 2007, saltcedar transpiration was measured on eight plants at Slitherin from July 20-September 2; five plants at Diablo East from June 22-July 8; and seven plants at Swamp from June 20-July 17 (reported in [8]). In 2008, saltcedar transpiration was measured on eight plants at Diablo Tower from August 8-August 16; 11 plants at Diablo Southwest from July 3-July 18; and 10 plants at Hot Springs. At the end of each measurement period, gauged branches were harvested and brought to the Environmental Research Laboratory in Tucson, Arizona, for determination of leaf dry weight and leaf area per branch.

Calculation of sap flux requires a correction for conductive heat loss that occurs in the absence of sap flux, which is usually accomplished by assuming that sap flux goes to zero between 2–4 am each day, and using temperature readings during those hours as zero points. However, saltcedar is now known to transpire at night [8,43]. Therefore, at the end of each sap flux measurement period, we continued to measure temperatures for two hours after harvesting the branch above the point where the sensor was attached, and those temperature values were used as zero points for calibrating sensors.

2.3. Scaling ET_{actual} to Whole Plants and Stands of Plants Based on Leaf Area Index

Sap flow data were collected in units of grams of water transported per hour through a gauged branch. Data were converted to volume of water loss per m^2 of leaf area (E_L), canopy area (E_C) or ground area (E_G) per day, expressed as mm d^{-1} of water loss over an indeterminate surface area. For comparison with stomatal conductance over diurnal cycles, E_L was also expressed as mmol H_2O m^{-2} sec^{-1} [41,42].

To convert E to E_L, grams dry weight of leaves for each branch were converted to m^2 of leaf area by determining Specific Leaf Area (SLA) (m^2 one-sided leaf area per g dry weight of leaves) for fresh leaf samples from 10 different plants per site. Surface area was measured by placing fresh leaves flat

side down on a sheet of graph paper, then counting the number of grid intersections covered by leaves (the point intercept method). The area per grid multiplied by number of grid intersections covered gave the area covered by leaves. Then the leaves were dried in an oven (60 °C) to determine dry weight, and SLA per branch was used to calculate E_L. SLA for saltcedar was 0.0079 m^2 g^{-1} (SE = 0.0004). Methods are described in more detail in Nagler *et al.* [44].

To convert E_L to E_C, plant-specific leaf area index (LAPS) was measured within plant canopies over the plot area:

$$E_C = E_L \times LAPS \tag{3}$$

To covert E_L to E_G, LAI on a ground-area basis was calculated as:

$$LAI = LAPS \times f_c \tag{4}$$

where f_c is fractional vegetation cover and:

$$E_G = LAI \times E_L \tag{5}$$

We used a Licor LAI 2000 meter (Licor Inc., Lincoln, NE) to measure LAPS at 50–100 points within each plant stand, collecting readings in June, July and August, 2007 and 2008. We calibrated the Licor LAI 2000 readings against leaf harvest methods by recording LAPS by Licor LAI 2000 under selected canopies for which we also harvested leaves to determine LAPS [8]. We placed a 0.25 m^2 PVC plastic frame horizontally over the canopy at the point where LAPS was measured by Licor, then harvested all the leaves within the frame. The leaves from these quadrant samples were then dried and weighed, allowing us to express the sap flow results in terms of water loss per m^2 of canopy area, by making a ratio between the g leaves per sap flow branch and the g leaves per m^2 of canopy determined by the quadrant harvests. LAPS values measured by Licor LAI 2000 were multiplied by 0.84 to make them consistent with leaf-harvest LAPS values.

To calculate f_c, we used high resolution (1 m) aerial photographs collected by Chris Neale (Utah State University) in June, 2007. We measured f_c over an area of approximately 6 ha around each site, in order to extrapolate E_G to the footprint size of MODIS pixels, used to scale E_G over the floodplain. Each image was imported into a viewing program (Adobe Photoshop) and a grid (ca. 200 squares) was placed over the image. Each grid intersection was visually scored as either bare soil or vegetation (visible as false-color red from the NIR band in the photos). Visual scoring was used instead of a spectral classification method due to the presence of shadows, which interfered with spectral methods [34]. Since saltcedar made up > 90% of the vegetation at each site, E_G was based only on saltcedar transpiration rates.

2.4. Measurement of Alfalfa ET_actual

Alfalfa ET_{actual} was measured by soil moisture depletion using a neutron hydroprobe (503 DR Hydroprobe, Campbell Pacific Nuclear, Inc., Concord, CA) following methods in Bell [45] and Glenn *et al.* [46]. In 2006, five PVC (Schedule 40) neutron hydroprobe access tubes were installed 100 m from each of the four corners and in the center of the alfalfa field. The neutron hydroprobe was calibrated to convert counts per minute (cpm) to volumetric moisture content (cm^3 H_2O cm^{-3} soil). We determined bulk density by extracting soil cores near each hydroprobe port with a volumetric

soil-sampling auger. We then measured cpm at the 60 cm depth at each hydroprobe port. Soil moisture was determined in the laboratory on soil samples taken at each probe port at the same time and soil depth as neutron hydroprobe readings. Bulk density of the soil was 1.50 g cm^{-3}. The linear equation relating soil moisture to cpm was:

$$\text{Soil Moisture (cm}^3 \text{ H}_2\text{O cm}^{-3} \text{ soil)} = 0.0000467 \text{ cpm} - 0.0246 \ (r^2 = 0.998) \tag{6}$$

ET$_{actual}$ was estimated in August and September, 2006, and June, 2007, by measuring soil moisture content 48 hours after irrigation and then 6–7 days later at each probe port. The 48-hour delay in taking the initial reading allowed time for water to infiltrate into the soil profile, and for a soil crust to form to reduce surface evaporation. Soil moisture was measured at 0.3 m intervals from the 0.3 m soil depth to 1.8 m depth in the probe ports. The water table was encountered at about 1.8–2.0 m depth.

2.5. MODIS Data

MODIS data from the Terra satellite are collected on a near-daily basis and are processed and composited into 16-day values by NASA's EROS Data Center, using 3–5 cloud-free images for each collection interval [47]. Both the Normalized Difference Vegetation Index (NDVI) and the Enhanced Vegetation Index (EVI) are available as georectified and atmospherically corrected products with a resolution of 250 m. We used EVI instead of the more commonly used NDVI because previous studies [17] showed that ET$_{actual}$ measured at 11 moisture flux tower sites was significantly better correlated with MODIS EVI than NDVI (see also [9]). EVI is calculated as:

$$\text{EVI} = 2.5 \times (\rho\text{NIR} - \rho\text{Red})/(1 + \rho\text{NIR} + (6 \times \rho\text{Red} - 7.5 \times \rho\text{Blue})) \tag{7}$$

where the coefficient "1" accounts for canopy background scattering and the blue and red coefficients, 6 and 7.5, minimize residual aerosol variations. We converted EVI to a full scale between 0 and 1 (EVI*):

$$\text{EVI*} = 1 - (\text{EVI}_{max} - \text{EVI})/(\text{EVI}_{max} - \text{EVI}_{min}) \tag{8}$$

where EVI$_{max}$ is the value for full plant cover and EVI$_{min}$ is the value for bare soil. We used values of 0.542 and 0.091, respectively, from a large data set collected over three western riparian zones in a previous study [7]. We used a scaled value of EVI following the recommendation of Choudhury *et al.* [18], but they noted that regression equations can also be developed using unscaled vegetation indices. Also, our value for maximum EVI was based on riparian canopies in a previous study [7] and alfalfa had EVI* values greater than 1.0 (EVI was not scaled separately for each vegetation type).

MODIS EVI data were obtained from the Oak Ridge National Laboratory DAAC site [47]. This site allows the user to view the footprint of a MODIS pixel or set of pixels displayed on a current, high-resolution Google Earth image before a final selection is made. We used this feature of the ORNL DAAC site to ensure that pixels encompassed our areas of interest (e.g., sap flow sites and the alfalfa field), and were not contaminated by adjacent land cover types. For the sap flow sites, a single pixel centered around each site was selected. For the alfalfa field, three adjacent pixels, each wholly contained within the field, were selected. The 16-day period or periods encompassing the dates of ground ET$_{actual}$ collection were obtained.

2.6. Meteorological Data and Other Calculations

Meteorological data for CNWR and the Hayday Farms alfalfa field were obtained from the Parker, Arizona, AZMET station [35]. Data for saltcedar and arrowweed at Havasu National Wildlife Refuge (HNWR) were from the Mojave #2 AZMET station [35]. Two formulations of ET_o were used to calculate ET_oF by Equation (2). The first was the FAO-56 formula for reference crop ET_o using the Penman Monteith equation (ET_{o-PM}) (see [19,48] for a description of the meteorological variables, instrumentation and calculation procedures). This is generally the preferred formula for ET_o since it includes all the major variables affecting ET_{actual}. However, since it is formulated for a short grass-reference crop under light winds, it is dominated by the radiation term in the Penman Monteith equation, which might not be applicable to riparian vegetation [16]. The Blaney Criddle formulation of ET_o (ET_{o-BC}) is based on mean monthly temperature and mean daily percentage of annual daytime hours [49], and over the range of latitudes in the present study it is dominated by temperature, which affects D and is the advective term in the Penman Monteith equation [48]. A previous study [50] found a much better correlation between flux tower ET_{actual} and ET_{o-BC} than ET_{o-PM}. Also, temperature data is much more widely available than the full set of meteorological data needed to calculate ET_{o-PM}. In Arizona, for example, there are nearly 500 cooperative NOAA stations reporting temperature and precipitation throughout the state, but only 27 AZMET reporting ET_{o-PM}. We calculated ET_{o-BC} by the formula in Brouwer and Heibloem [49] using AZMET mean monthly temperature:

$$ET_{o-BC} = p \times (0.46T_{mean} + 8) \tag{9}$$

where p is mean daily percentage of annual daytime hours (from a table in Brouwer and Heibloem [49], T_{mean} is mean monthly temperature in ^{o}C, and ET_{o-BC} is in units of mm d^{-1}.

Canopy conductance (G_S) on a leaf-area basis (mmol m^{-2} s^{-1}) was calculated by the formula [41,42]:

$$G_S = E_L/D \times K_G \text{ (10)} \tag{10}$$

where K_G is the stomatal or canopy conductance coefficient (kPa), calculated from atmospheric pressure corrected for temperature effects by the formula:

$$K_G = 115.8 + 0.4226T \tag{11}$$

The term $E_L/D \times K_G$ is the ratio of transpiration to atmospheric water demand, and it is related to the degree of stomatal opening at a given time of day [48].

For unstressed crops, diurnal patterns of E_L closely follow the net radiation (R_n) curve, and the evaporative fraction (EF) is generally constant during the daylight hours [6,51,52]:

$$EF = \lambda E_G/R_n \tag{12}$$

where λE_G is the latent heat of evaporation (W m^{-2}) calculated from hourly values of E_G measured by sap flow sensors, assuming a heat of evaporation of 2,257 kJ kg^{-1} water [48]. Hourly values of R_n were calculated as 0.77 R_s measured at the Parker AZMET station, assuming an albedo of 0.23 [19]. Equation 12 is used to scale instantaneous estimates of ET_{actual}, made using thermal bands on satellites at midday, to daily time steps [6,52]. Diurnal plots of EF can also be used to diagnose stress effects on photosynthesis and stomatal conductance [53,54]. Estimates of saltcedar E_G from E_L, LAPS and f_c in Equation 5 are susceptible to propagation errors due to separate errors in estimating each term in the

equation [55]. The propagation error was calculated based on the standard error the mean of each variable using software in [56].

2.7. Other Sources of E_G and ET_{actual} Data

In addition to the data collected here, the final ET_{actual} algorithm based on Equations 1 and 2 contained additional published data collected for riparian plants on the Lower Colorado River. Two years of saltcedar data and one year of arrowweed data were collected at HNWR, in which ET_{actual} was measured by Bowen Ratio moisture flux towers [7,30]. One year of E_G data were collected by sap flow sensors for cottonwood at CNWR in 2005 [38]. One year of E_G and G_S data were collected by sap flow sensors at three different saltcedar sites than those in the present study at CNWR in 2007 [8]. For these sites, summer ET_{actual} or E_G values were matched with single MODIS pixels encompassing each site, and EVI* and ET_oF over each measurement period were calculated.

3. Results

3.1. Meteorological, Soil and Aquifer Conditions at Saltcedar and Alfalfa Sites

Diurnal temperature, vapor pressure deficit, and radiation curves from the Parker AZMET station over the 2007 and 2008 sap flow measurement periods (June-August), are in Figure 2.

Figure 2. Climate conditions measured at the Parker, Arizona, AZMET station during periods in which sap flow measurements were made at Cibola National Wildlife Refuge in 2007 (closed circles) and 2008 (open circles). Values are means over the June-August measurement intervals of air temperature (A), vapor pressure deficit (B), and solar radiation (R_S) (C).
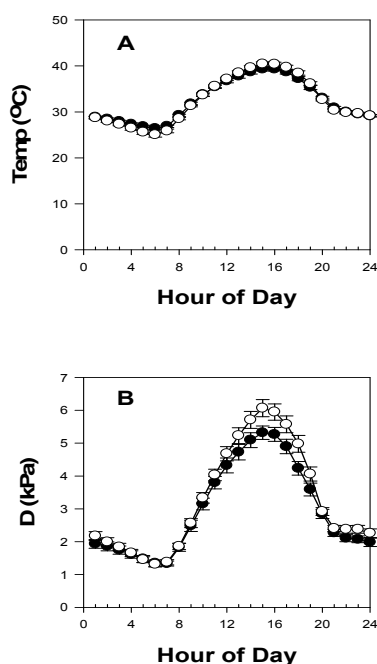
Figure 2. *Cont*.
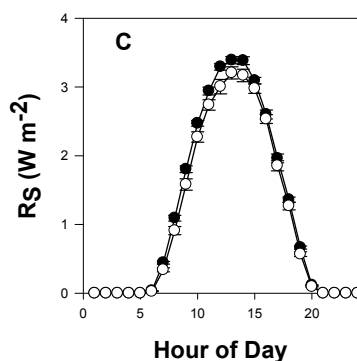
Conditions were similar both years, characterized by bright, hot days with very high midday atmospheric water demand. Rainfall over the measurement periods was 2.0 mm in 2007 and 8.8 mm in 2008. Sites differed in soil properties, depth to water, and salinity of the aquifer (Table 1). Soils at Swamp and Slitherin were loams, whereas soils at Diablo Tower, Diablo Southwest, Diablo East and Hot Springs were sands. The water table was deeper at Slitherin (3.5 m) than at the other saltcedar sites (2.4–2.8 m). Aquifer salinities ranged from 3.90 dS m^{-1} at Swamp to 24.0 dS m^{-1} at Dialbo Southwest and salinity increased in direct proportion to distance from the active channel (r^2 = 0.82. P = 0.005). The equation of best fit was:

$$EC \ (dS \ m^{-1}) = 0.012 \ d - 0.626 \tag{13}$$

where EC is electrical conductivity and d is distance from the river in meters. A value of 1.41 dS m^{-1} for river water was used as the zero distance value. Aquifer temperatures were markedly elevated at Hot Springs due to the intrusion of geothermal water into the aquifer. The alfalfa field had a clay loam soil, and an elevated, non-saline aquifer due to the effect of irrigation.

3.2. LAPS, f_c, E_L, and E_G of Saltcedar Stands

LAPS varied from 2–4 among saltcedar sites (Figure 3A) but did not vary significantly (P > 0.05) from June to August at a given site [8]. f_c varied from 0.47–0.95 (Figure 3B). E_L (Figure 3C) and E_G (Figure 3D) was markedly lower at Hot Springs than at other sites. We attribute this to the elevated aquifer temperatures. Excluding Hot Springs, mean E_L was 2.30 mm d^{-1} and the coefficient of variation (CV) was 0.20; mean E_G was 5.35 mm d^{-1} and CV was 0.47. Over all sites, standard errors of E_L, LAPS and f_c were 4.7%, 2.1% and 0.7% of mean values, respectively, and the cumulative propagation error for E_G was 6.5% of the mean value across sites.

3.3. Diurnal Variation in E_L, G_S and EF

Saltcedar showed markedly different patterns of E_L and G_S among sites (Figure 4). Slitherin (Figure 4A) was the only site where E_L closely tracked the daily radiation curve (r^2 = 0.92, P < 0.001), with peak E_L at 1,200–1,300 hrs, and peak G_S at 1,000 hrs. The other sites had peak E_L well before 1,200, and afternoon E_L was truncated when compared to the radiation curve. Diablo East had peak E_L at 0800 hrs and peak G_S was at sunrise (0600 hrs) then dropped after 0800 hrs. All sites tended to show a recovery in G_S between 1,600 and sunset. All plants also continued E_L at night, with

nocturnal water loss accounting for 25% of total E_L across sites. The foliage of the plants was heavily coated with highly saline water droplets at dawn, even though temperatures were well above the dew point, indicating that much of the nighttime water loss could be due to guttation through salt glands on saltcedar leaves [57] rather than transpiration through stomata.

Diurnal curves of EF showed U shapes typical of crops, for which EF often exceeds 1.0 in early morning and late afternoon, when advective effects dominate ET_{actual}, but are less than 1.0 during midday hours, when ET_{actual} is limited by R_n, which supplies the energy needed to evaporate water [6,48,51,52]. However, patterns of saltcedar EF were not constant over the daylight hours at most of the sites (Figure 5). Morning values of EF (*i.e.*, 0800–1200 hrs) were 0.53 (SE = 0.065), compared to only 0.35 (SE = 0.019) in the afternoon (1,300–1,700 hrs) due to the midday depression of E_L and G_S across sites. Slitherin was the only site for which midday EF was in the range of 0.8–1.0, indicating the maximum utilization of available energy to support E_G, while the other sites ranged from 0.3–0.5.

Figure 3. Saltcedar plant-specific leaf area index (LAPS) (A), fractional cover (B), leaf-area transpiration (C) and ground-area transpiration (D) at six sites at Cilobla National Wildlife Refuge on the Lower Colorado River.
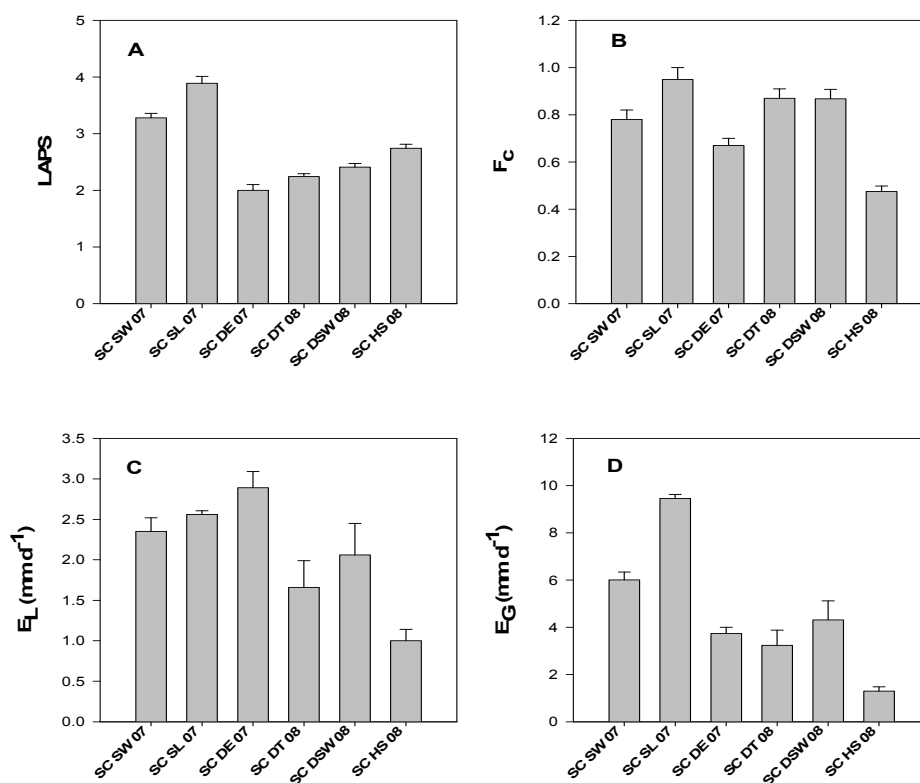
Figure 4. Leaf-area transpiration (E_L) (closed circles) and stomatal conductance (G_S) (open circles) of saltcedar at six sites at Cibola National Wildlife Refuge on the Lower Colorado River. Results are hourly mean values over each measurement period. Error bars are standard errors. Horizontal white rectangles above the x-axis denotes daylight hours.
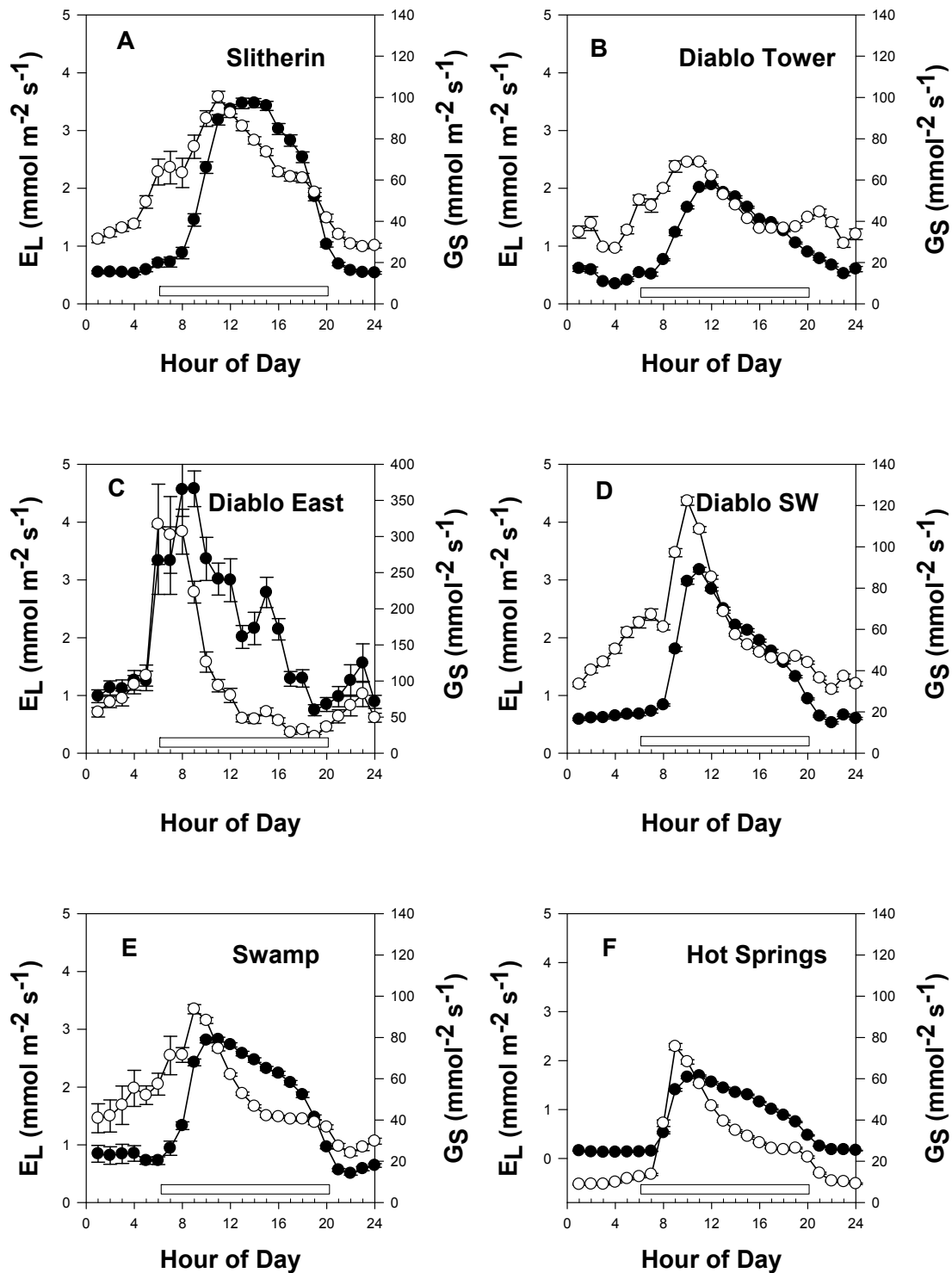
Figure 5. Evaporative fraction (EF), defined as ET_{actual}/R_n, for saltcedar at six sites at Cibola National Wildlife Refuge on the Lower Colorado River. Sites are Slitherin (closed circles), Swamp (open circles), Diablo Tower (closed triangles), Diablo Southwest (open triangles), Hot Springs (closed squares) and Diablo East (open squares).
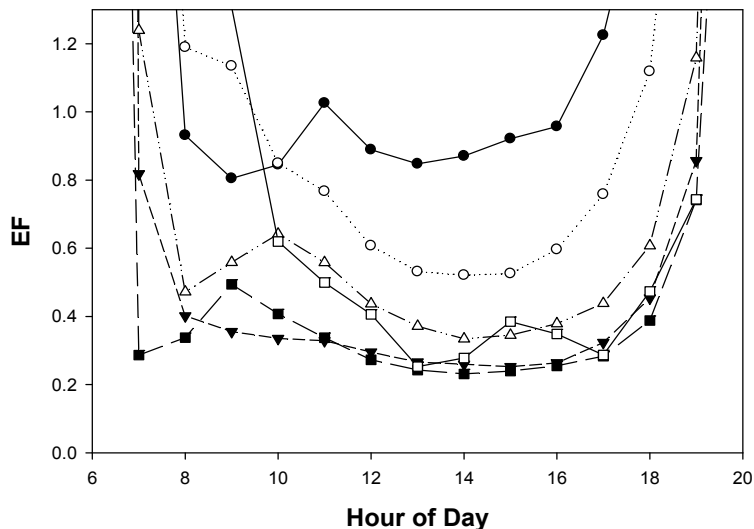
3.4. Alfalfa ET_{actual}

ET_{actual} measurements were made when plants were 30–50 cm tall and had not been recently cut. LAI measured by Licor LAI 2000 during the June, 2007 measurement period was 4.42 (Std. Error = 0.42). Soil moisture depletion in units of cm^3 cm^{-3} d^{-1} were converted to ET units (mm H_2O d^{-1}) based on water loss in the top 1.8 m of soil profile. ET_{actual} in the alfalfa field ranged from 6.96 mm d^{-1} at the end of September, 2006, to 8.77 m d^{-1} in early June, 2007 (Figure 6). The standard error of mean ET_{actual} tended to be high at each sample date, due to variation in ET_{actual} among the five sites within the field. However, differences in soil moisture content at the two sampling dates in each measurement period were significant across soil depths and probe ports for all measurement periods ($P < 0.05$).

Figure 6. Alfalfa ET_{actual} at a field in the Palo Verde Irrigation District calculated from the difference in soil moisture levels measured 48 hours after an irrigation (closed circles) and 6–7 days latter (open circles). Each data point is the mean of five probe measurements. SE is the standard error of ET_{actual} over all five ports. P is the probability that mean moisture contents across soil depths are equal at the two measurement intervals by paired t-test.

Figure 6. *Cont.*

August 18 - 25, 2006

September 26 - October 1, 2006
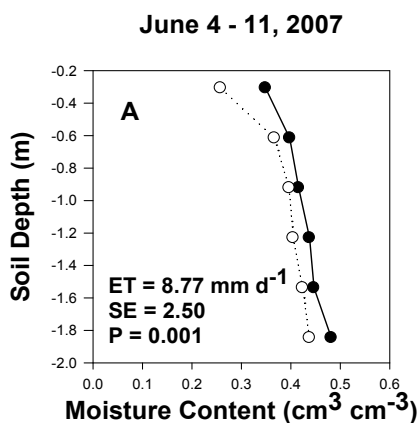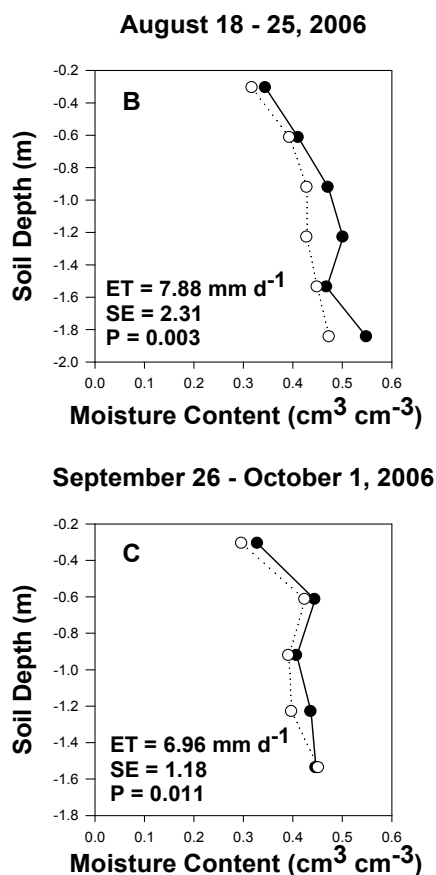
3.5. Linear Equations for E_GF and ET_oF Based on EVI*

For the eight saltcedar data points (six sites at CNWR and two years data at one site at HNWR), the correlation between E_G or ET_{actual} and EVI* was significant (P = 0.036) but of low predictive power (r^2 = 0.55). We attempted to improve and generalize the algorithm by normalizing E_G data to reference crop ET_o, and by including other plant types. Hot Springs was not included in the regression equations as it was clearly an outlier due to the elevated aquifer temperatures. Linear regression equations between ET_oF and EVI* were significant for both ET_{o-BC} and ET_{o-PM} (P < 0.01), but y-intercepts were small and non-significant (P = 0.69 and 0.84, respectively). This is expected because the scaling procedure sets EVI* for bare soil at 0. Therefore, it was justified to pass regression equations through the origin to determine the final algorithms (Figure 7). ET_{o-BC} (Figure 7A) clearly gave a better fit of data than ET_{o-PM} (Figure 7B). The standard error of the mean increased with increasing ET_oF, as expected for regression through the origin. At ET_oF = 1.0, the error around the mean for the expression using ET_{o-BC} was about 20%, compared to 25% for ET_{o-PM}. When only saltcedar ET_oF was used in the regression with EVI*, the slope of the ET_oF:EVI* equation based on ET_{o-BC} was 1.20, nearly the same as when all plants were included (1.22) (no significant difference in slopes at P = 0.05), hence the equation in Figure 7A can be used to estimate ET_oF for either saltcedar or mixed stands of agricultural and riparian plants on the Lower Colorado River.

Figure 7. Ratio of ET$_{actual}$ or E$_G$ to reference crop ET (ET$_o$F) for plants on the Lower Colorado River, using the Blaney Criddle method (A) and the Penman Monteith method (B) for ET$_o$. Plants and locations are: saltcedar at Slitherin (SL), Swamp (SW), Diablo East (DE), Diablo Southwest (DSW) and Diablo Tower (DT) at Cibola National Wildlife Refuge (closed circles); saltcedar at Hot Springs at Cibola National Wildlife Refuge (cross); saltcedar at Havasu National Wildlife Refuge in 2002 and 2003 (open triangles); arrowweed at Havasu National Wildlife Refuge in 2003 (closed square); and alfalfa at Palo Verde Irrigation District on three dates (open circles). Hot Springs was not included in the regression analyses. Regression equations were passed through the origin and dashed lines denote 95% confidence intervals. Error bars are standard errors of means.

ET$_o$F Based on Blaney Criddle ET$_O$

ET$_o$F Based on Penman Monteith ET$_O$
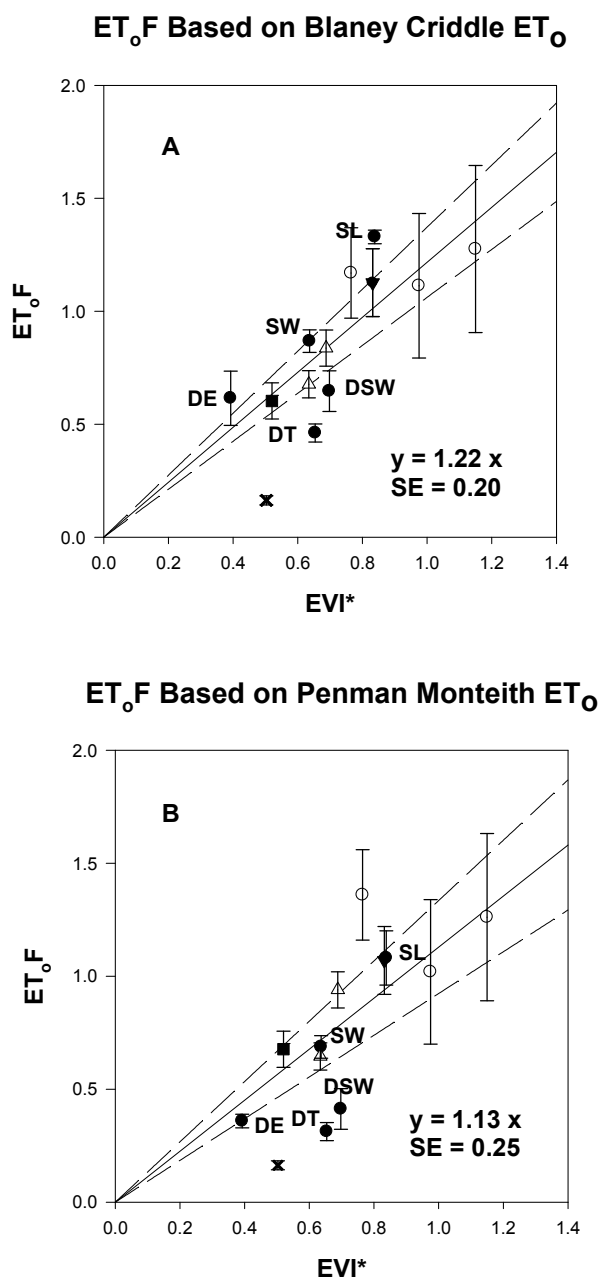
The reason for the better performance of $ET_{o\text{-}BC}$ compared to $ET_{o\text{-}PM}$ was further investigated with flux tower data for saltcedar at HNWR (from data in [7]). Over an annual cycle, $ET_{o\text{-}BC}$ was about 10% lower than $ET_{o\text{-}PM}$ and they had slightly different seasonal curves, with the temperature-driven $ET_{o\text{-}BC}$ lagging behind the radiation-driven $ET_{o\text{-}PM}$ in the spring (Figure 8). Saltcedar loses its leaves in winter and does not green up until mid-March, and when flux tower data for saltcedar ET_{actual} was plotted against ET_o, its phenology better matched $ET_{o\text{-}BC}$ than $ET_{o\text{-}PM}$ (Figure 8).

Figure 8. ET_o calculated by the Penman Monteith method ($ET_{o\text{-}PM}$), the Blaney Criddle method ($ET_{o\text{-}BC}$) and saltcedar ET_{actual} measured by Bowen ratio moisture flux towers at Havasu National Wildlife Refuge on the Lower Colorado River in 2002 and 2003. Data are from [7]. Correlation coefficients (r) between each variable are shown under the curves.
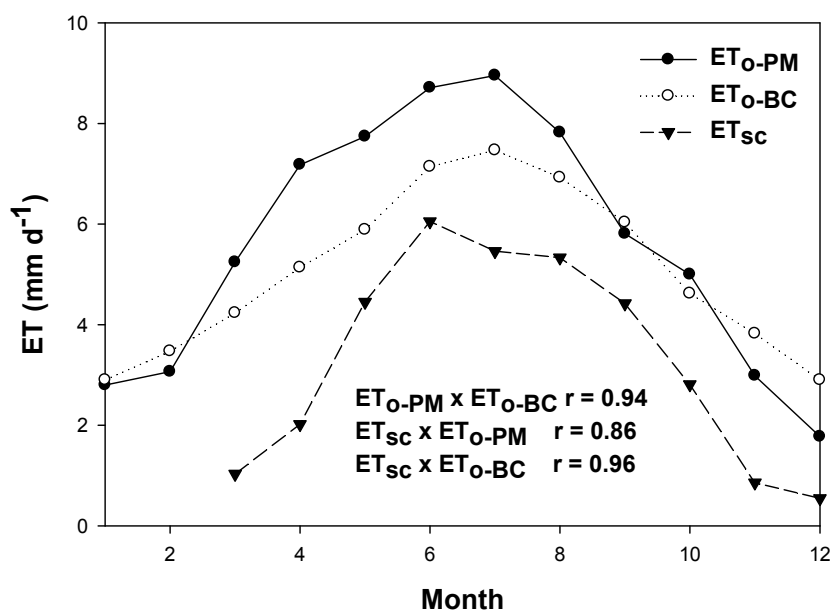
4. Discussion

4.1. Diurnal Patterns of Saltcedar E_L, G_S and EF Indicate Stress

The study site at CNWR was selected as typical of the dense saltcedar stands that have developed on wide river terraces on the Lower Colorado River. Due to lack of overbank flooding, the aquifer has become salinized, and it is dominated by saltcedar and native salt tolerant shrubs. The aquifer is replenished by underflow from the river, and the salinity of the aquifer increases in proportion to distance from the river, due to extraction of water by saltcedar while most of the salts remain in the aquifer [8,34].

Except at Slitherin, diurnal patterns of E_L and G_S were not at all typical of unstressed crop plants. At the other sites, saltcedar exhibited marked midday depression of E_L and G_S, a characteristic of stressed plants [21]. Furthermore, the response was not uniform among sites; in fact, saltcedar at each site exhibited different diurnal patterns of E, G_S and EF. Peak E_L at Slitherin was at 1,200 hrs, whereas plants at Diablo East had peak E_L at 0800 hours and the other sites were intermediate. Other studies have also noted midday depression of saltcedar ET_{actual} [31,58-60].

Saltcedar at Hot Springs was obviously affected by high temperatures in the aquifer. However, the factors controlling E_L and E_G at the other sites were not as clearcut. Depth to the aquifer did not seem to be a controlling factor, since the aquifer was deepest at Slitherin, which had the highest values of LAPS, f_c and E_G. High salinity might have negatively affected plants at Diablo and Diablo SW, but Slitherin outperformed plants at Swamp, Diablo East and Hot Springs, despite having similar salinities as those sites.

Soil conditions in the aquifer differed among sites and could be responsible for differences in diurnal responses. E_L and E_G of phreatophytes can be profoundly affected by soil texture, which regulates the rate at which roots can extract water from the aquifer [61]. Sands (as at Hot Springs, Diablo Tower, Diablo Southwest and Diablo East) have low matric potential, and water in the rhizosphere can cavitate above a critical level of E_L, limiting transpiration rates in sandy aquifers [62]. On the other hand, heavier soils as at Slitherin can support higher rates of E_L due to less tendency for the water column to cavitate at the soil-root interface [62]. A working hypothesis, which we have not yet tested, is that the soil in the root zone of saltcedar recharges with water at night, but is depleted faster than it can be replenished in the morning, leading to midday depression of saltcedar E_L at the sites with sandy soils. This could lead to the observed patterns in which morning EF was much higher than afternoon EF at all sites except Slitherin. In support of this hypothesis, E_G was negatively correlated with % sand (r = −0.612) and positively correlated with % clay (r = 0.543) (P > 0.05, not significant, for each), and a multiple linear regression between E_G and % sand and % clay had r = 0.91 (significant at P = 0.029), despite the small sample size (6 sites).

Unlike most crop plants [63], saltcedar has high rates of nocturnal water loss, amounting to 25% of total consumptive use in this study and even more in a study on the Middle Rio Grande [43]. Part of this water loss was due to guttation of liquid water rather than E_L. Guttation of water through salt glands is functional in disposing of excess salts from the leaf apoplast [57].

4.2. Remote Sensing Algorithm for Scaling ET*actual*

Given the diverse physiological responses of saltcedar at different sites, caution is needed in using remote sensing methods to scale riparian ET*actual* over wide areas. With respect to SEB methods, the assumption of constant EF over daylight hours was not met for saltcedar. A midday snapshot of ET*actual* by satellite would tend to underestimate daily ET*actual*, and the error would vary from site to site and with the timing of the satellite overpass. With respect to VI methods, E_L was not constant on a daily time step, but varied from 1.66–2.89 mm m^{-2} d^{-1} among sites (excluding Hot Springs, which was 1.0 mm m^{-2} d^{-1}). Hence, an ET*actual* estimate based on the assumption of a constant relationship between E_L and ET$_o$ (e.g., [1]) would not accurately project ET*actual* at any given site. In aggregate, however, ET$_o$F from saltcedar sites plotted against EVI* fell along the same line as alfalfa, arrowweed and cottonwood. Midday depression of saltcedar E_L was compensated by nighttime transpiration and guttation, and a generalized algorithm for scaling ET*actual* over mixed scenes had an error term of about 20% (mean ET*actual* = 6.2 mm d^{-1}, SEM = 1.2) when ET$_{o-BC}$ was used for reference ET. This is within the accuracy range of other remote sensing methods for ET*actual*, which have error rates of 15–30% when compared to ground measurements [14,16]. Hence, the algorithm developed here was within the accuracy range of other methods, and appears to be valid for scaling ET*actual* over the Lower

Colorado River. However, the existence of sites such as Hot Springs, which had aberrant values of E_G in relation to EVI*, suggests that the ecophysiological constraints on E_G should be characterized by ground studies in a biome of interest, before remote sensing methods are used to scale physiological functions such as E_G.

4.3. Comparison with Other Remote Sensing Methods for ET

Nagler *et al.* [7,50] developed a similar VI method for riparian ET_{actual}, in which time-series flux tower ET_{actual} data were regressed against EVI* from MODIS and meteorological data collected at the flux tower sites. In those studies maximum daily temperature had the most explanatory power among meteorological variables, and addition of other variables did not improve the regression equation. The present results support that study, in that ET_{o-BC} (largely driven by temperature) had more explanatory power than ET_{o-PM} (largely driven by radiation) [16]. Desert agricultural and riparian ET_{actual} rates can be enhanced by advective effects from the surrounding arid landscape, which increases with increasing temperatures (discussed in [16]). Saltcedar ET_{actual} rates projected for CNWR based on methods in [7] are about 20% higher than those projected in this study [34], perhaps due to the use of flux tower data in [7] versus primarily sap flow data in this study. Flux tower data includes both bare soil evaporation and transpiration while sap flow only measures transpiration.

Most remote sensing methods for estimating ET_{actual} have used thermal data from satellite sensors to solve the surface energy balance (SEB) [14,15,64], and several of these have been developed as commercial products [65,66]. Most of these methods require high-resolution thermal imagery (e.g., from Landsat satellites), which have reduced temporal resolution compared to MODIS. Gonzalez-Dugo *et al.* [6] found similar levels of accuracy of daily ET_{actual} predictions for a VI/crop coefficient method based on FAO-56 [19] and SEB methods based on thermal NIR satellite bands. However, the sources of error were different. SEB methods were affected by the assumption of constant EF, needed to scale instantaneous measurements to daily values, and by differences in calibrating radiometric temperatures to give aerodynamic surface temperatures. On the other hand, the VI method was unable to detect early signs of water stress, whereas SEB methods detect stress as an increase in sensible heat flux at a given value of vegetation cover. Since saltcedar plots in this study exhibited variable degrees of stress, SEB methods could conceivably give a more accurate spatial depiction of ET_{actual} over a floodplain than simple VI methods. Time-series VI methods based on MODIS can provide the primary ET_{actual} data needed in constructing agricultural and riparian water budgets, but these should be augmented by high-resolution SEB methods for detecting stress at the level of individual agricultural fields or stands of riparian plants in western riverine irrigation districts. A combined approach would provide the information needed to monitor consumptive water use and improve water use efficiency of managed and natural vegetation in these districts.

4.4. Sources of Error and Uncertainty

Remote sensing estimates of ET_{actual} are subject to a number of sources of error and uncertainty, as already noted. The main sources of error in this study are outlined below:

A. Several methods were used to measure ET_{actual} on the ground, including sap flow sensors, flux towers, and neutron probe water balance measurements. Each of these havs their own, separate,

sources of measurement and scaling errors, and they do not strictly measure the same thing. Sap flow sensors measure plant transpiration while towers and hydroprobe methods measure total ET_{actual}.

B. The sample size and duration of measurements unavoidably varied among plant types. Single alfalfa, cottonwood and arrowweed sites were measured, whereas six sites were measured for saltcedar. Sap flow sensors measure plant water use over a period of weeks, compared to years for tower measurements. Hence, A and B introduce uncertainty into the ground measurements used to calibrate remote sensing algorithms. These errors are in the range of 10–40% across methods and depend in part on the skill of the practicioners (reviewed in [67]).

C. Vegetation index methods for ET_{actual} cannot account for stress effects, which proved to be substantial and to differ across different plant stands for saltcedar. A strength of the algorithm developed in this study was that it could be applied across different plant types, because even high-resolution satellite imagery cannot resolve the different riparian and agricultural plants present in mixed landscapes on western rivers. However, pooling of crop types inevitably obscures likely difference in transpiration efficiency and other physiological factors that affect leaf-level transpiration rates, thereby introducing additional uncertainty into the remote sensing estimates.

D. The resolution of the imagery and other scaling issues also introduce uncertainty into the estimates. MODIS pixels encompass 6 ha and often contain mixed cover types, but they offer the advantage of high temporal resolution, with near daily coverage. On the other hand, Landsat and other higher resolution images, used in other studies (e.g., [1,6]), leave gaps of weeks or months between measurements.

On balance, the present method offers sufficient accuracy to improve our estimates of ET_{actual} over the range of crops and climatic conditions for which it was calibrated, but does not provide a general algorithm for ET_{actual} for other applications. Fortunately, there are now hundreds of ground stations collecting ET_{actual} data in different biome types around the world [16,17] and these can provide local calibration of empirical remote sensing methods such as the one described here.

5. Conclusions

This study developed a computation method for estimating ET_{actual} using time-series satellite-derived vegetation index values from MODIS, calibrated with ground measurements of ET_o and ET_{actual}. The resulting algorithm for ET_{actual} had an error or uncertainty of about 20%, within the range of other remote sensing methods for ET_{actual}, and allowed ET_{actual} to be scaled across irrigation districts and riparian areas on the Lower Colorado River (see [68]). Similar locally calibrated and validated algorithms can be developed for other applications for which frequent-return satellite imagery and ground meteorological and ET_{actual} data are available. These applications can reduce the error bars around the ET component of basin-wide hydrological models and aid in understanding plant water use across wide areas.

Acknowledgements

References and Notes

1. Groeneveld, D.P.; Baugh, W.M.; Sanderson, J.S.; Cooper, D.J. Annual groundwater evapotranspiration mapped from single satellite scenes. *J. Hydrol.* **2007**, *344*, 146-156.
2. Glenn, E.; Morino, K.; Didan, K.; Jordan, F.; Nagler, P.; Waugh, J.; Carroll, K.; Sheader, L. Scaling sap flux measurements of grazed and ungrazed shrub communities with fine and coarse-resolution remote sensing. *Ecohydrol.* **2008**, *1*, 316-329.
3. Nagler, P.L.; Glenn, E.P.; Kim, H.; Emmerich, W.; Scott, R.L.; Huxmam, T.E.; Huete, A.R. Relationship between evapotranspiration and precipitation pulses in a semiarid rangeland estimated by moisture flux towers and MODIS vegetation indices. *J. Arid. Environ.* **2007**, *70*, 443-462.
4. Hunsaker, D.J.; Fitzgerald, G.J.; French, A.N.; Clarke, T.R.; Ottman, M.J.; Pinter, P.J. Wheat irrigation management using multispectral crop coefficients. I. Crop evapotranspiration prediction. *Trans. ASABE* **2007**, *50*, 2017-2033.
5. Kim, J.Y.; Hogue, T.S. Evaluation of a MODIS-based potential evapotranspiration product at the point scale. *J. Hydrometeor.* **2008** *9*, 444-460.
6. Gonzalez-Dugo, M.P.; Neale, C.M.U.; Mateos, L.; Kustas, W.P.; Anderson, M.C.; Li, F. A comparison of operational remote-sensing based models for estimating crop evapotranspiration. *Agr. Forest Meteor.* **2009**, *49*, 2082-2097.
7. Nagler, P.; Scott, R.; Westenburg, C.; Cleverly, J.; Glenn, E.; Huete, A. Evapotranspiration on western US rivers estimated using the Enhanced Vegetation Index from MODIS and data from eddy covariance and Bowen ratio flux towers. *Remote Sens. Environ.* **2005**, *97*, 337-351.
8. Nagler, P.L.; Morino, K.; Didan, K.; Osterberg, J.; Hultine, K.; Glenn, E. Wide-area estimates of saltcedar (Tamarix spp.) evapotranspiration on the lower Colorado River measured by heat balance and remote sensing methods. *Ecohydrol.* **2009**, *2*, 18-33.
9. Juarez, R.I.N.; Goulden, M.L.; Myneni, R.B.; Fu, R.; Bernardes, S.; Gao, H. An empirical approach to retrieving monthly evapotranspiration over Amazonia. *Int. J. Remote Sens.* **2008**, *29*, 7045-7063.
10. Leuning, R.; Zhang, Y.Q.; Rajaud, A.; Cleugh, H.; Tu, K. A simple surface conductance model to estimate regional evapotranspiration using MODIS leaf area index and the Penman-Monteith equation. *Water Resour. Res.* **2008**, *44*, Article No. W10419.
11. Zhang, Y.Q.; Chiew, F.H.S.; Zhang, L.; Leuning, R.; Cleugh, H.A. Estimating catchment evaporation and runoff using MODIS leaf area index and the Penman-Monteith equation. *Water Resou. Res.* **2008**, *44*, Article No. W10420.
12. Mu, Q.; Heinsch, F.A.; Zhao, M.; Running, S.W. Development of a global evapotranspiration algorithm based on MODIS and global meteorology data. *Remote Sens. Environ.* **2007**, *111*, 519-536.
13. Wang, K.C.; Liang, S.L. An improved method for estimating global evapotranspiration based on satellite determination of surface net radiation, vegetation index, temperature, and soil moisture. *J. Hydrometeor.* **2008**, *9*, 712-727.
14. Kalma, J.D.; McVicar, T.R.; McCabe, M.F. Estimating land surface evaporation: a review of methods using remotely sensed surface temperature data. *Surv. Geophys.* **2008**, *29*, 421-469.

15. Kustas, W.; Norman, J. Use of remote sensing for evapotranspiration monitoring over land surfaces. *Hydrologic. Sci. J.* **1996**, *41*, 495-516.

16. Glenn, E.; Huete, A.; Nagler, P.; Hirschboek, K.; Brown, P. Integrating remote sensing and ground methods to estimate evapotranspiration. *Crit.Rev. Plant Sci.* **2007**, *26*, 139-168.

17. Glenn, E.; Huete, A.; Nagler, P.L.; Nelson, S.G. Relationship between remotely-sensed vegetation indices, canopy attributes and plant physiological processes: what vegetation indices can and cannot tell us about the landscape. *Sensors* **2008**, *8*, 2136-2160.

18. Choudhury, B.J.; Ahmed, N.U.; Idso, S.B.; Reginato, R.J.; Daughtry, C.S.T. Relations between evaporation coefficients and vegetation indexes studied by model simulations. *Remote Sens. Environ.* **1994**, *50*, 1-17.

19. Allen, R.; Pereira, L.; Rais, D.; Smith, M. *Crop Evapotranspiration—Guidelines for Computing Crop Water Requirements—FAO Irrigation and Drainage Paper 56*; Food and Agriculture Organization of the United Nations: Rome, Italy, 1998.

20. Mata-Gonzalez, R.; McLendon, T.; Martin, D.W. The inappropriate use of crop transpiration coefficients (K_c) to estimate evapotranspiration in arid ecosystems. *Arid Land Res. Manag.* **2005**, *19*, 285-295.

21. Xu, D.; Shen, Y. External and internal factors responsible for midday depression of photosynthesis. In *Handbook of Photosynthesis*, 2nd ed.; Pessarakli, M., Ed.; Taylor & Francis: Boca Raton, FL, USA, 2005; pp. 297-298.

22. Gaskin, J.; Schaal, B. Hybrid Tamarix widespread in US invasion and undetected in native Asian range. *P. Nat. Acad. Sci.USA* **2002**, *99*, 11256-11259.

23. Glenn, E.; Nagler, P. Comparative ecophysiology of *Tamarix ramosissima* and native trees in western US riparian zones. *J. Arid Envir.* **2005**, *61*, 419-446.

24. Stromberg, J.; Chew, M.; Nagler, P.L.; Glenn, E.P. Change perceptions of change: the role of scientists in Tamarisk and river management. *Restor. Ecol.* **2009**, *17*, 177-186.

25. Di Tomaso, J. Impact, biology, and ecology of saltcedar (*Tamarix* spp.) in the southwestern United States. *Weed Technol.* **1998**, *12*, 326-336.

26. Zavaleta, E. The economic value of controlling an invasive shrub. *Ambio* **2000**, *29*, 462-467.

27. United States 109th Congress. *HR 2720: Salt Cedar and Russian Olive Control Demonstration Act*; United State Congress: Washington, DC, USA, 2009.

28. Devitt, D.; Sala, A.; Smith, S.; Cleverly, J.; Shaulis, L.; Hammett, R. Bowen ratio estimates of evapotranspiration for *Tamarix ramosissima* stands on the Virgin River in southern Nevada. *Water Resour. Res.* **1998**, *34*, 2407-2414.

29. Cleverly, J.; Dahm, C.; Thibault, J.; McDonnell, D.; Coonrod, J. Riparian ecohydrology: regulation of water flux from the ground to the atmosphere in the Middle Rio Grande, New Mexico. *Hydrol. Process.* **2006**, *20*, 3207-3225.

30. Westenberg, C.; Harper, D.; DeMeo, G. *Evapotranspiration by Phreatophytes Along the Lower Colorado River at Havasu National Wildlife Refuge, Arizona*; US Geological Survey Scientific Investigations Report, 2006-5043; USGS: Henderson, NV, USA, 2006.

31. Sala, A.; Smith, S.; Devitt, D. Water use by *Tamarix ramosissima* and associated phreatophytes in a Mojave Desert floodplain. *Ecol. Appl.* **1996**, *6*, 888-898.

32. Owens, M.; Moore, G. Saltcedar water use: Realistic and unrealistic expectations. *Rangeland Ecol. Manag.* **2007**, *60*, 553-557.

33. Huete, A.; Didan, K.; Miura, T.; Rodriquez, E.; Gao, X.; Ferreira, L. Overview of the radiometric and biophysical performance of the MODIS vegetation indices. *Remote Sens. Environ.* **2002**, *83*, 195-213.

34. Nagler, P.; Glenn, E.; Didan, K.; Osterberg, J.; Jordan, F.; Cunningham, J. Wide-area estimates of stand structure and water use of *Tamarix* spp. on the Lower Colorado River: implications for restoration and water management projects. *Restor. Ecol.* **2009**, *16*, 136-145.

35. AZMET. *The Arizona Meteorological Network*; University of Arizona: Tucson, AZ, USA, 2009. Available online: http://cals.arizona.edu/azmet/ (accessed on November 18, 2009).

36. Grime, V.; Sinclair, F. Sources of error in stem heat balance sap flow measurements. *Agr. Forest Meteor.* **1999**, *94,* 103-121.

37. Kjelgaard, J.; Stockle, C.; Black, R.; Campbell, G. Measuring sap flow with the heat balance approach using constant and variable heat inputs. *Agr. Forest Meteor.* **1997**, *85*, 239-250.

38. Nagler, P.; Glenn, E.; Thompson, T. Comparison of transpiration rates among saltcedar, cottonwood and willow trees by sap flow and canopy temperature methods. *Agr. Forest Meteor.* **2003**, *116*, 73-89.

39. Nagler, P.; Jetton, A.; Fleming, J., Didan; K., Glenn; E., Erker, J.; Morino, K.; Milliken, J.; Gloss, S. Evapotranspiration in a cottonwood (*Populus fremontii*) restoration plantation estimated by sap flow and remote sensing methods. *Agr, Forest Meteor.* **2007**, *144*, 95-110.

40. Scott R.; Huxman, T.; Cable, W.; Emmerich, W. Partitioning of evapotranspiration and its relation to carbon dioxide exchange in a Chihuahuan Desert shrubland. *Hydrol. Process.* **2006**, *20*, 3227-3243.

41. Phillips, N.; Oren, R. A comparison of daily representations of canopy conductance based on two conditional time-averaging methods and the dependence of daily conductance on environmental factors. *Ann. Sci. Forest.* **1998**, *55*, 217-235.

42. Ewers, B.; Oren, R. Analyses of assumptions and errors in the calculation of stomatal conductance from sap flux measurements. *Tree Physiol.* **2000**, *20*, 579-589.

43. Moore, G.; Cleverly, J.; Owens, M. Nocturnal transpiration in riparian *Tamarix* thickets authenticated by sap flux, eddy covariance and leaf gas exchange measurements. *Tree Physiol.* **2008**, *28*, 521-528.

44. Nagler, P.; Glenn, E.; Thompson, T.; Huete, A. Leaf area index and Normalized Difference Vegetation Index as predictors of canopy characteristics and light interception by riparian species on the Lower Colorado River. *Agr. Forest Meteor.* **2004**, *116*, 103-112.

45. Bell, J.P. *Neutron Probe Practice. Institute of Hydrology Report 19*; Institute of Hydrology: Oxfordshire, UK, 1987.

46. Glenn, E.P.; McKeon, C.; Gerhart, V.; Nagler, P.L.; Jordan, F.; Artiola, J. Deficit irrigation of a landscape halophyte for reuse of saline waste water in a desert city. *Landscape Urban Plan.* **2009**, *89*, 57-64.

47. Oak Ridge National Laboratory Distributed Active Archive Center (ORNL DAAC). *MODIS Subsetted Land Products, Collection 5*; ORNL DAAC: Oak Ridge, TN, USA. Available online: www.daac.ornl/MODIS/modis.html (accessed on November 18, 2009).

48. Monteith, J.; Unsworth, M. *Principles of Environmental Physics*, 2nd ed.; Edward Arnold: London, UK, 1990.

49. Brouwer, C.; Heibloem, M. *Irrigation Water Management Training Manual No. 3*; FAO: Rome, Italy, 1986.

50. Nagler, P.L.; Cleverly, J.; Glenn, E.; Pampkin, D.; Huete, A.; Wan, Z.M. Predicting riparian evapotranspiration from MODIS vegetation indices and meteorological data. *Remote Sens. Environ.* **2005**, *94*, 17-30.

51. Crago, R.D. Conservation and validity of the evaporative fraction during the daytime. *J. Hydrol.* **1996**, *180*, 173-180.

52. Chavez, J.L.; Neale, C.M.; Prueger, J.H.; Kustas, W.P. Daily evapotranspiration estimates from extrapolating instantaneous airborne remote sensing ET values. *Irrig. Sci.* **2008**, *27*, 67-81.

53. Wilson, K.; Balodocchi, D.; Falge, E.; Aubinet, M.; Berbigier, P.; Bernhofer, C.; Dolman, H.; Field, C.; Goldstein, A.; Granier, A.; Hollinger, D.; Katul, G.; Law, B.; Meyers, T.; Moncreiff, J.; Monson, R.; Tenhunen, J.; Valentini, R.; Verma, S.; Wofsy, S. Diurnal centroid of ecosystem energy and carbon fluxes at FLUXNET sites. *J. Geophys. Res.-Atmos.* **2003**, *108*, Art. No. 4664.

54. Mackay, D.S.; Samanta, S.; Nemani, R.R.; Band, L.E. Multi-objective parameter estimation for simulating canopy transpiration in forested watersheds. *J. Hydrol.* **2003**, *277*, 230-247.

55. Bevington, P. *Data Reduction and Error Analysis for the Physical Sciences*; McGraw-Hill Inc.: New York, NY, USA, 1969.

56. GraphPad Inc. GraphPad QuickCalcs. Available online: www.graphpad.com/quickcalcs/ ErrorPropplusminus/cfm (accessed on November 18, 2009).

57. Bosabalidis, A.M.; Thomson, W.W. Ultrastructural development and secretion in the salt-glands of *Tamarix aphylla* L. *J. Ultra. Res.* **1985**, *92*, 55-62.

58. Horton, J.; Hart, S.; Kolb, T. Physiological condition and water source use of Sonoran Desert riparian trees at the Bill Williams River, Arizona, USA. *Isot. Environ. Health S.* **2003**, *39*, 69-82.

59. Horton, J.; Kolb, T.; Hart, S. Physiological response to groundwater depth varies among species and with river flow regulation. *Ecol. App.* **2001**, *11*, 1046-1059.

60. Horton, J.; Kolb, T.; Hart, S. Responses of riparian trees to interannual variation in ground water depth in a semi-arid river basin. *Plant Cell Environ.* **2001**, *24*, 293-304.

61. Hultine, K.; Koepke, D.; Pockman, W.; Fravolini, A.; Sperry, J.; Williams, D. Influence of soil texture on hydraulic properties and water relations of a dominant warm-desert phreatophyte. *Tree Physiol.* **2006**, *26*, 313-323.

62. Sperry, J.; Adler, F.; Campbell, G.; Comstock, J. Limitation of plant water use by rhizosphere and xylem conductance: results from a model. *Plant Cell Environ.* **1998**, *21*, 347-359.

63. Snyder, K.; Richards, J.; Donovan, L. Night-time conductance in C3 and C4 species: do plants lose water at night? *J. Exp. Bot.* **2003**, *54*, 861-865.

64. Su, Z. The Surface Energy Balance System (SEBS) for estimation of turbulent heat fluxes. *Hydrol. Earth Syst. S.* **2002**, *6*, 85-99.

65. Allen, R.; Tasumi, M.; Trezza, R. Satellite-based energy balance for mapping evapotranspiration with internalized calibration (METRIC)—Model. *J. Irrig. Drain. E-ASCE* **2007**, *133*, 380-394.

66. Bastiaanssen, W.G.M.; Noordman, E.J.M.; Pelgrum, H.; Davids, G., Thoreson, B.P.; Allen, R.G. SEBAL model with remotely sensed data to improve water-resources management under actual field conditions. *J. Irrig. Drain. E-ASCE* **2005**, *131*, 85-93.

67. Tamarisk Coalition. *Independent Peer Review of Tamarisk and Russian Olive Evapotranspiration Colorado River Basin*; Tamarisk Coalition: Grand Junction, CO, USA, 2009. Available online: http://www.tamariskcoalition.org/tamariskcoalition/PDF/ET%20Report%20FINAL%204-16-09% 20(2).pdf (accessed on December 1, 2009).

68. Murray, R.S.; Nagler, P.L.; Morino, K.; Glenn, E.P. An empirical algorithm for estimating agricultural and riparian evapotranspiration using MODIS Enhanced Vegetation Index and ground measurements of ET. II. Application to the Lower Colorado River, US. *Remote Sens.* **2009**, *1*, 1125-1138.